ACS Sustainable Chemistry & Engineering

Research Article

pubs.acs.org/journal/ascecg

Thiamine-Based Nitrogen, Phosphorus, and Silicon Tri-doped Carbon for Supercapacitor Applications

Sunil Kumar Ramasahayam,* Zachary Hicks, and Tito Viswanathan*

Department of Chemistry, University of Arkansas at Little Rock, 2801 S. University Ave, Little Rock, Arkansas 72204, United States

Supporting Information

ABSTRACT: This paper reports the synthesis of N, P, and Si tri-doped C (NPSiDC) using thiamine (a renewable resource material), silicone fluid, and ammonium polyphosphate. A one-pot microwave assisted method was utilized in synthesizing NPSiDC. The method is simple, rapid, and economical which does not employ any inert or reducing gases. Three variants of NPSiDCs were synthesized by varying the proportions of the precursor materials. NPSiDC-1 was found to have high specific surface area of 471 m^2 g^{-1} and a single point total pore volume of 0.25 cm^3 g^{-1}. Raman spectroscopy results revealed the presence of defects in an sp^2 C lattice. XPS analysis revealed the presence of N, P, Si, and O in C. NPSiDC-1 and NPSiDC-2 exhibited tremendous potential for supercapacitor applications with NPSiDC-1 recording highest specific capacitance value of 318 F g^{-1} in 6 M KOH. NPSiDCs were discovered to be electrochemically stable after 2000 cycles in 6 M KOH.

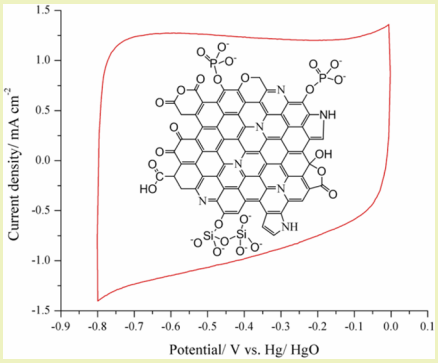

KEYWORDS: *Thiamine, Microwave, Economical, Defects, Capacitance*

INTRODUCTION

Increasing energy demands coupled with diminishing fossil fuel reserves propel the need for sustainable, efficient energy generation and storage technologies. Supercapacitors are the front-runners for energy storage owing to their long charge−discharge life, low equivalent series resistance, and power density.[1] Supercapacitors are also superior to traditional batteries and capacitors, for they can be made from renewable resource materials and produce little to no toxic waste in its construction. By combining the high energy density of batteries and high power density of capacitors, supercapacitors have become a superior means for energy storage. Different classes of materials are being utilized for supercapacitor applications among which metal oxides,[2] conducting polymers,[3] and porous carbons[4] are worth mentioning.

Metal oxides such as RuO_2, MnO_2, NiO, etc., face conductivity issues and are expensive,[5] whereas conducting polymers suffer from short cycling life.[3,6] Therefore, recently porous carbon materials are gaining increasing importance for supercapacitor applications due to their low cost, abundance, good conductivity, uniform porosity, high surface area, and electrochemical stability.[7] Porous carbon materials have unique surface chemical structures that contribute to energy storage through pseudocapacitance by facilitating electron transfer reactions at the electrode−electrolyte interface.[8] They also possess unique electronic structure which facilitate energy storage by electrical double layer capacitance.[3] However, they suffer from tortuous porosity which impedes energy storage capabilities.[9] Doping with heteroatoms like N, B, S, etc., is believed to enhance energy storage capabilities of porous carbon materials by improving the chemical and electronic structure of carbon based materials.[6] Previous studies have shown how heteroatom doped carbons can produce high capacitance values. Yang et al. reported N and P codoped carbon synthesized by electrospinning of polyacrylonitrile with phosphoric acid followed by thermal treatments, which yielded a capacitance of 224.9 F g^{-1} at 0.5 A g^{-1} in 1 M H_2SO_4.[10] Another study by Qiu et al. also reported high capacitance values (154.4 F g^{-1}) by heteroatom doping with N and P codoped microporous carbon developed by carbonizing phosphoric acid doped polyaniline.[11] Also, dual doping of heteroatoms (N and P) was found to synergistically enhance the electrochemical performance of doped carbon materials compared to single doped or undoped counterparts.[11] Doping with hetero atoms breaks the electro neutrality of carbon and creates electrochemically active sites.[12] These defect sites themselves may catalyze some fast faradaic redox reactions or enhance the electrical double layer formation.[12] Porous carbon materials with well-defined pores (micropores, mesopores and macropores) are required to facilitate ion transport and charge accumulation for better energy storage performance.[13,14]

Different techniques exist today to synthesize porous carbon materials, for example, chemical vapor deposition, thermal annealing, plasma radiation, pyrolysis, etc., to name a few.[15−21] However, these techniques make use of longer synthesis durations, involve toxic chemicals, and are expensive.[15] We report a novel one-pot microwave assisted method to develop doped carbon materials for energy storage. The reported

Received: May 21, 2015
Revised: June 29, 2015
Published: July 12, 2015

DOI: 10.1021/acssuschemeng.5b00453
ACS Sustainable Chem. Eng. 2015, 3, 2194−2202

synthesis technique does not employ any toxic or reducing gases, is high yielding, involves shorter synthesis durations (30 min), and is environmentally friendly.[22−26]

We report the synthesis of a novel N, P, and Si doped carbon (NPSiDC) from thiamine hydrochloride using ammonium polyphosphate as the dehydrating agent. Thiamine (vitamin B1) is a natural product obtained from a variety of plant and animal sources such as yeast, pork, and legumes, which are considered as rich sources of the vitamin. Ammonium polyphosphate is used as a dehydrating agent and a source for N and P dopants. The synthesized material was extensively studied by different characterization techniques and investigated for supercapacitor applications.

EXPERIMENTAL SECTION

Materials. Thiamine hydrochloride was purchased from Acros Organics, New Jersey. Silicon fluid 500 cst was obtained from Clearco Products Co., Inc., Bensalem, PA. Ammonium polyphosphate was obtained from JLS Chemical Inc., China. Potassium hydroxide and sulfuric acid were purchased from Fischer Scientific, New Jersey. Polytetrafuoroethylene was purchased from Sigma Aldrich, St. Louis. Ethanol was purchased from Fischer Scientific, New Jersey. All the chemicals obtained were of analytical grade and were utilized without further purification.

Synthesis. NPSiDCs were prepared by a novel microwave-assisted technique. A predetermined amount of silicone fluid and ammonium polyphosphate were mixed in a boron nitride crucible to which a suitable proportion of thiamine hydrochloride was added and mixed thoroughly. The mixture of precursor materials were subjected to microwave irradiation in a Panasonic Household Microwave Oven (Model No. NN-H965WFX) operating at 2.45 GHz and 1.25 kW power for a duration of 30 min. As microwave heating is rapid, temperatures greater than 1000 °C were expected to be attained during the initial 1−2 min of microwave duration.[27] Under such extreme temperatures, dehydration and eventual carbonization of precursor materials occur. After 30 min of microwave heating, the carbonized material was allowed to cool in the microwave oven cavity for 2 h after which the product was recovered. By varying the amounts of precursor materials, three different kinds of NPSiDCs were developed. The amounts of precursor materials utilized in developing NPSiDCs and the products recovered are summarized in Table 1. Figure 1 illustrates the reaction between precursor materials and the proposed general structure of NPSiDC.

Table 1. Summary of Amounts of Precursor Materials Utilized and Average Product Obtained from Syntheses of NPSiDCs

sample	thiamine (g)	silicone fluid (g)	ammonium polyphosphate (g)	product (g)
NPSiDC-1	1.0	0.15	0.20	0.17 ± 0.04
NPSiDC-2	1.0	0.30	0.40	0.23 ± 0.11
NPSiDC-3	1.0	0.60	0.80	0.23 ± 0.06

Characterization Methods. The morphology of NPSiDCs was studied using JEOL 7000F scanning electron microscope. Surface area and porosity characteristics were determined using Micromeritics surface area analyzer ASAP-2020 by nitrogen (N_2) sorption studies at a bath temperature of 77.3 K. To identify the chemical nature of carbon, Raman spectra were recorded using a Horiba Jobin Yvon LabRam 800 equipped with 784 nm He−Ne laser. Surface elemental composition and chemical bonding environments of different elements was investigated using Thermo K-alpha X-ray photoelectron spectrometer (source Al Kα radiation, 1486 eV, 12 kV, spot size 200 μm, and carbon internal standard at 284.8 eV). Bulk conductivity values of the doped carbon samples were estimated by a "four point probe method" using a Keithley 224 current source and a Keithley 617 electrometer employing van der Pauw equation.[28] Doped carbon samples were mixed with 20% polytetrafluoroethylene (PTFE) and pressed into a pellet using a hydraulic press at 15 000 psi for 1 min. The measurements were recorded at three different spots on pellet prepared from each sample and an average of observed conductivity values has been reported. Bulk conductivity values were computed using the following equation:

$$\sigma = \frac{\ln 2}{\pi t}\frac{i}{V}$$

where σ is bulk conductivity (S cm^{-1}), i is applied current (A), V is the voltage drop (V), and t is the thickness of the pellet (cm).

Electrochemical Methods. All electrochemical measurements were recorded using a AFCBP1 bipotentiostat from Pine Instrument Company. A three electrode system comprising of a glassy carbon working electrode (5 mm diameter and 0.196 cm^2 geometric area)

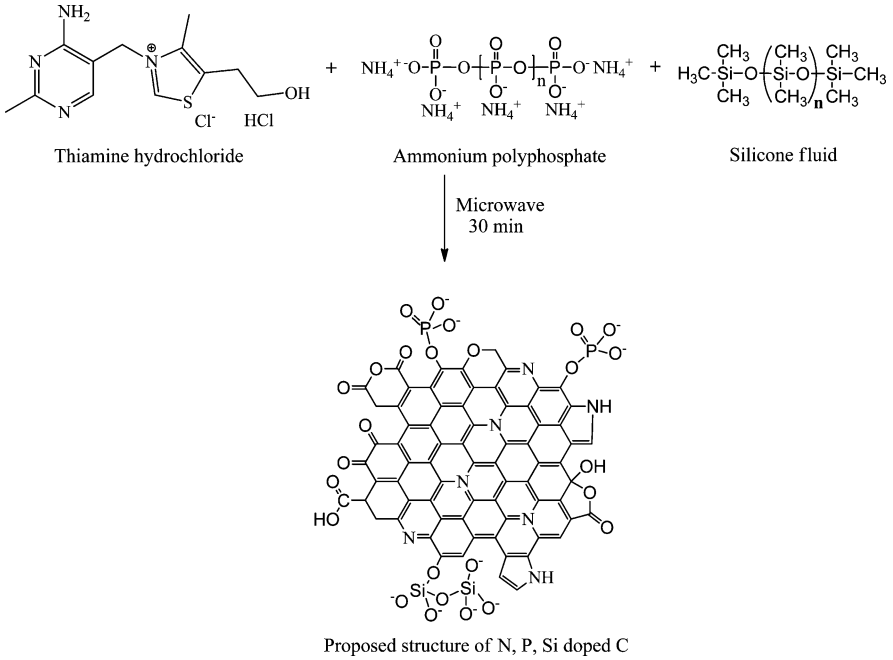

Figure 1. Proposed general structure of NPSiDC synthesized from thiamine hydrochloride, ammonium polyphosphate, and silicone fluid.

DOI: 10.1021/acssuschemeng.5b00453
ACS Sustainable Chem. Eng. 2015, 3, 2194−2202

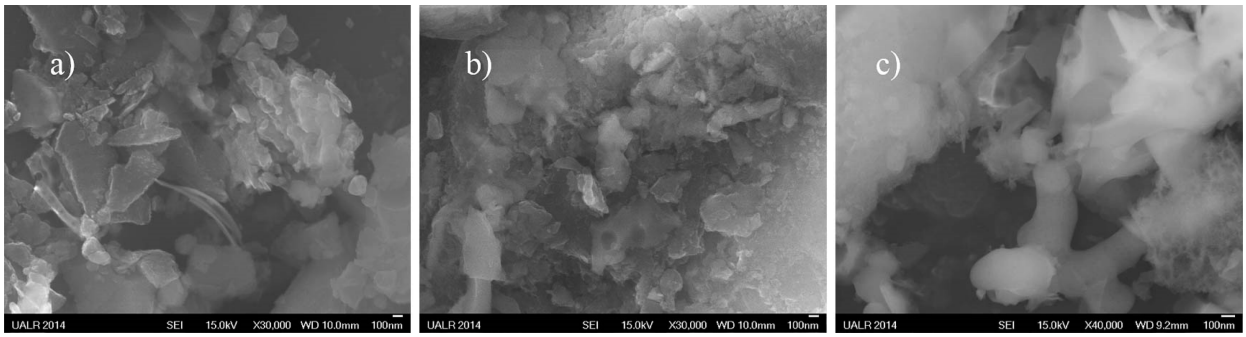

Figure 2. SEM images of (a) NPSiDC-1, (b) NPSiDC-2, and (c) NPSiDC-3.

enclosed in a polytetrafluoroethylene holder, a Ag/AgCl reference electrode (in aqueous 1 M H_2SO_4), a Hg/HgO reference electrode (in aqueous 6 M KOH), and a Pt counterelectrode was used for all electrochemical experiments. The electrolytic solution was saturated with N_2 for at least 1 h before the measurements and a continuous N_2 flow above the electrolyte was maintained to minimize interference from O_2. The glassy carbon electrode surface was cleaned using 0.05 μ alumina polish followed by rinsing with distilled water. A 90:5:5 mass ratio of suspension of NPSiDC material, carbon black and polytetrafluoroethylene (PTFE) in 1 mL ethanol was prepared using ultrasound for 2 h. A 10 μL sample of the prepared catalyst suspension was drop-casted onto glassy carbon electrode, air-dried, followed by an additional 10 μL, air-dried, and finally dried in a vacuum oven. Cyclic voltammograms were recorded at scan rates ranging from 5 to 100 mV s^{-1} in a potential range of 0 to 800 mV in 1 M H_2SO_4 and −800 to 0 mV in 6 M KOH. Galvanostatic charge−discharge studies were performed at a current density of 0.2 A g^{-1} in 6 M KOH using a three electrode system comprising of glassy carbon working electrode, Hg/HgO reference electrode and Pt counter electrode.

Specific capacitance (C_s) and interfacial capacitance (C_i) values were calculated from cyclic voltammograms using the following equations:

$$C_s = \int i(\mathrm{d}V)/Vm\upsilon = Q/\Delta Vm = \int i\mathrm{d}t/\Delta Vm = i\Delta t/\Delta Vm$$

$$C_{s,\mathrm{total}} = (C_{\mathrm{anode}} + C_{\mathrm{cathode}})/2 \quad (1)$$

and

$$C_i = (C_{s,\mathrm{total}}/S_{\mathrm{BET}}) \quad (2)$$

where i is the current density, V is the potential applied, Q is the charge generated, m is the mass of the active material, υ is the potential scan rate, and S_{BET} is the surface area of the active material determined by BET method.

RESULTS AND DISCUSSION

Scanning Electron Microscopy (SEM). Scanning electron microscopic images of NPSiDCs can be seen in Figure 2. All NPSiDCs exhibit several irregular flake-like structures with diameters ranging from 100 nm to several hundred nanometers.

Surface Area and Porosity Analysis. The N_2 adsorption−desorption isotherms of NPSiDCs can be seen in Figure 3. All isotherms follow similar shapes and can be classified as Type IV according to IUPAC classification.[29] The hysteresis can be classified as type H4 according to IUPAC classification, which indicates no limiting adsorption at higher relative pressures and confirms the presence of slit shaped pores.[29] The sharp rise in the adsorption curves at lower relative pressure of 0.1−0.2 is due to monolayer adsorption, indicative of micropores. The almost linear middle portion is due to multilayer adsorption and the hysteresis between adsorption branch and desorption branch of the isotherms is indicative of capillary condensation

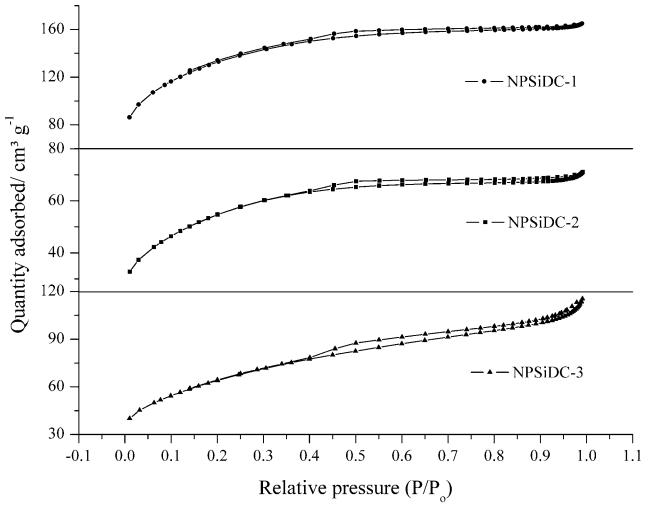

Figure 3. N_2 adsorption and desorption isotherms of NPSiDCs.

in mesopores.[30] The hysteresis in NPSiDC-3 is more pronounced than in NPSiDC-2, which is more pronounced than in NPSiDC-1. An interesting feature observed in NPSiDC-1 is the nonclosure point of the steep region of desorption branch at lower relative pressures. This is due to the irreversible interaction between N_2 and the adsorbent. The almost linear uptake at higher relative pressures indicates the presence of macropores. Table 2 summarizes the surface area and porosity

Table 2. Surface Area and Porosity Characteristics of NPSiDCs

sample	BET surface area (m^2 g^{-1})	micropore volume (cm^3 g^{-1})	mesopore volume (cm^3 g^{-1})	total pore volume (cm^3 g^{-1})	average pore diameter (Å)
NPSiDC-1	471.04	0.05	0.20	0.25	27.92
NPSiDC-2	228.34	0.01	0.14	0.15	34.24
NPSiDC-3	231.28	0.01	0.16	0.17	38.75

results of NPSiDCs. NPSiDC-1, NPSiDC-2, and NPSiDC-3 have specific surface areas of 471.04, 228.34, and 231.28 m^2 g^{-1}, respectively, calculated by the BET method. Figure 4 shows the pore size distribution of NPSiDCs with the inset showing pore size distribution up to 10 nm. It is evident from the curves that all NPSiDCs have different kinds of pores with majority of them distributed in the mesoporous region. It is noteworthy that a small hump can be seen in inset of Figure 4 for NPSiDC-2 at around 3.5 nm. The development of diverse pores can be attributed to the liberation of reducing gases from the precursor

DOI: 10.1021/acssuschemeng.5b00453
ACS Sustainable Chem. Eng. 2015, 3, 2194−2202

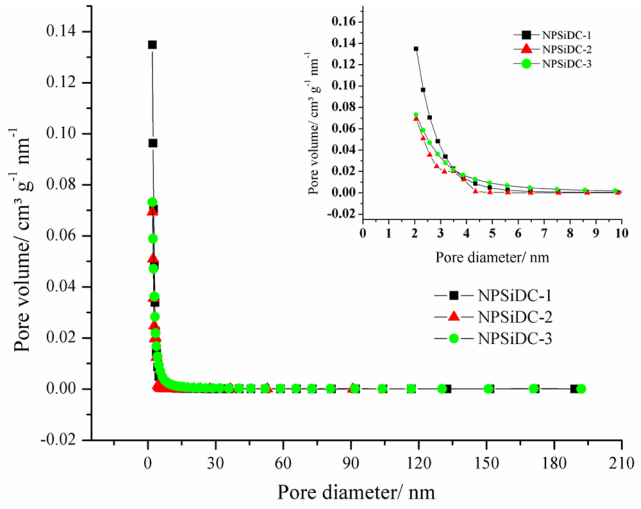

Figure 4. Pore size distribution of NPSiDCs with inset showing the pore size distribution up to 10 nm.

materials during the microwave treatment process. The presence of different kinds of pores is critical for energy storage applications as macropores and mesopores are involved in forming ion buffering reservoirs and decreasing ion transportation distance while micropores are involved in energy storage.[1,30,31]

X-ray Photoelectron Spectroscopy. XPS survey scan analyses have been performed on three different spots for each NPSiDC to investigate the surface elemental composition. Table 3 summarizes the average surface elemental composition results of NPSiDCs. All NPSiDCs predominantly contain C, O, and Si on the surface while N and P are present in minor quantities. NPSiDCs were expected to contain S along with the other mentioned elements but surprisingly negligible amounts of S was detected. The reason for this could be the low amount of S in thiamine (only one atom of S per molecule of thiamine) and also most of the S could be lost during the carbonization process. Figures S1−S6 represent the XPS survey spectra and region spectra recorded on one spot on NPSiDC samples.

Narrow scan analysis has also been performed on three different spots on each NPSiDC sample and no significant differences in the results obtained from the region spectra recorded at each spot were observed. Therefore, the results from only one representative scan for NPSiDC-1, NPSiDC-2, and NPSiDC-3 are presented in Tables 4, 5, and 6, respectively. All NPSiDCs have C 1s existing in six different environments indicated by fitted peaks at 284.7, 285.6 ± 0.2, 286.5, 287.8 ± 0.1, and 291.2 eV due to graphitic/sp^2 C−C,[32] sp^3 C−C/C−H,[33] C−O/C−N,[4,34] C═O/N−C═N,[16,33] and $\pi-\pi^*$ shakeup peak, respectively.[35] O in NPSiDCs exist mainly in two different bonding environments. The O 1s bonding environment at 533.2 ± 0.3 and 533.6 ± 0.6 eV in NPSiDC-2 and NPSiDC-3 can be attributed to C−O[36] and C−OH,[37] respectively; whereas, NPSiDC-1 exhibits O 1s bonding environments at 530.8 and 533.1 eV which can be attributed to quinone[36] and C−O, respectively.[15,36] Nitrogen in NPSiDC-1, NPSiDC-2, and NPSiDC-3 exists in two bonding environments at 399.1 ± 0.1 and 401.3 eV which can be attributed to pyridinic (and/or pyrrolic)[38,39] and graphitic/quarternary N, respectively.[33,37,40−42] Phosphorus in all PNDCs exists as P−O species represented by peak at 135 ± 0.7 eV with a doublet arising due to P $2p^{3/2}$ and P $2p^{1/2}$ spin states which is evidenced by a peak area ratio of 2:1.[15,36,37,40] Si fitted peak in NPSiDCs at 104 ± 0.5 eV (existing as a doublet due to Si $2p^{3/2}$ and Si $2p^{1/2}$ spin states which is evidenced by a peak area ratio of 2:1) can be attributed to Si−O bonding.[43] The presence of these different

Table 3. XPS Surface Elemental Composition of NPSiDCs

sample	carbon % (1s)	oxygen % (O 1s)	silicon % (Si 2p)	nitrogen % (N 1s)	phosphorus % (P 2p)
NPSiDC-1	56.78 ± 0.41	28.73 ± 0.22	10.00 ± 0.14	2.15 ± 0.01	2.34 ± 0.06
NPSiDC-2	30.54 ± 1.59	46.55 ± 0.98	17.34 ± 0.73	1.92 ± 0.08	3.65 ± 0.11
NPSiDC-3	27.14 ± 0.10	54.17 ± 0.54	17.25 ± 0.63	0.56 ± 0.02	0.88 ± 0.02

Table 4. Atom Percent and Bonding Environments of C, O, N, Si, and P in NPSiDC-1

element	At % (BE, eV)	element	At % (BE, eV)	element	At % (BE, eV)	element	At % (BE, eV)	element	At % (BE, eV)
C 1s scan A	49.21 (284.7)	O 1s scan A	98.18 (533.1)	N 1s scan A	81.40 (401.3)	Si 2p scan A	100 (103.9)	P 2p scan A	100.0 (134.3)
C 1s scan B	15.45 (285.4)	O 1s scan B	1.82 (530.8)	N 1s scan B	18.60 (399.1)				
C 1s scan C	11.55 (286.5)								
C 1s scan D	5.96 (287.7)								
C 1s scan E	5.06 (289.1)								
C 1s scan F	12.77 (291.2)								

Table 5. Atom Percent and Bonding Environments of C, O, N, Si, and P in NPSiDC-2

element	At % (BE, eV)	element	At % (BE, eV)	element	At % (BE, eV)	element	At % (BE, eV)	element	At % (BE, eV)
C 1s scan A	57.43 (284.7)	O 1s scan A	84.76 (533.2)	N 1s scan A	71.49 (401.3)	Si 2p scan A	100 (104.0)	P 2p scan A	100.0 (135.0)
C 1s scan B	8.88 (285.6)	O 1s scan B	15.24 (533.6)	N 1s scan B	28.51 (399.2)				
C 1s scan C	12.82 (286.5)								
C 1s scan D	6.11 (287.8)								
C 1s scan E	3.55 (289.2)								
C 1s scan F	11.21 (291.2)								

DOI: 10.1021/acssuschemeng.5b00453
ACS Sustainable Chem. Eng. 2015, 3, 2194−2202

Table 6. Atom Percent and Bonding Environments of C, O, N, Si, and P in NPSiDC-3

element	At % (BE, eV)	element	At % (BE, eV)	element	At % (BE, eV)	element	At % (BE, eV)	element	At % (BE, eV)
C 1s scan A	61.68 (284.7)	O 1s scan A	61.22 (533.5)	N 1s scan A	51.09 (401.3)	Si 2p scan A	100 (104.5)	P 2p scan A	100.0 (135.6)
C 1s scan B	8.88 (285.5)	O 1s scan B	38.78 (534.2)	N 1s scan B	48.91 (399.2)				
C 1s scan C	7.49 (286.5)								
C 1s scan D	7.09 (287.8)								
C 1s scan E	2.46 (289.3)								
C 1s scan F	12.39 (291.2)								

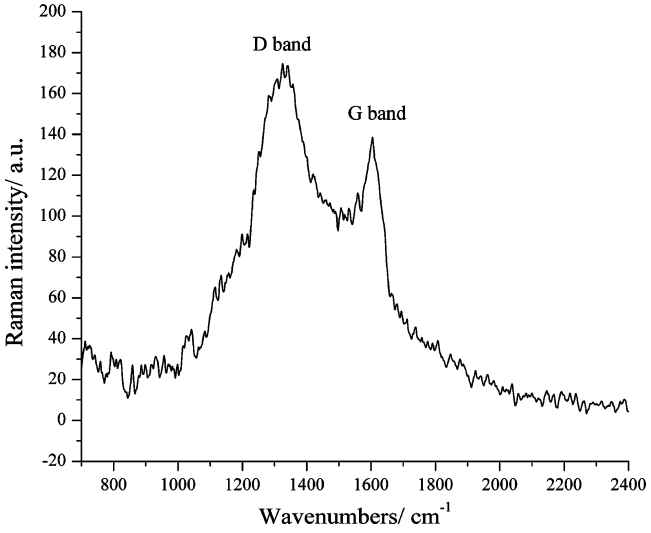

Figure 5. Raman spectra of NPSiDC-2 demonstrating the D band and the G band.

Table 7. Bulk Conductivity Values of NPSiDCs with 20% Binder

sample	binder (PTFE; wt %)	conductivity (S cm^{-1})
NPSiDC-1	20	0.027 ± 0.009
NPSiDC-2	20	0.003 ± 0.000
NPSiDC-3	20	0.000 ± 0.000

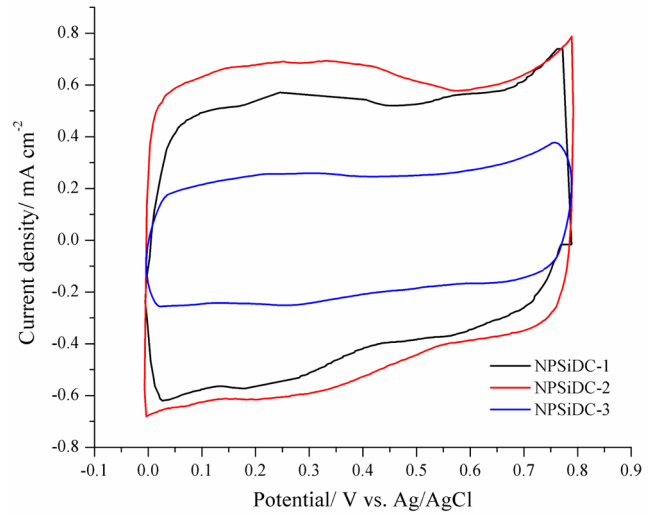

Figure 6. Cyclic voltammograms of NPSiDCs recorded in 1 M H_2SO_4 at a scan rate of 5 mV s^{-1}.

functionalities on the surface of NPSiDCs is expected to have a pronounced effect on their electrochemical performance.

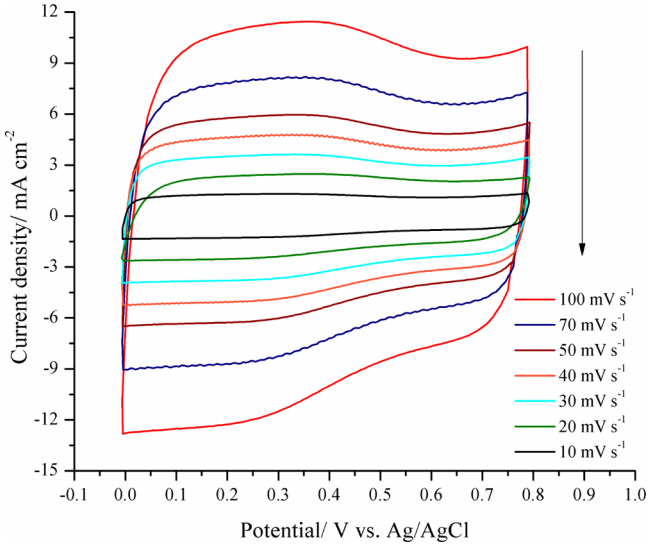

Figure 7. Cyclic voltammograms of NPSiDC-2 recorded at different scan rates in 1 M H_2SO_4.

Table 8. C_s and C_i Values of NPSiDCs in 1 M H_2SO_4 and 6 M KOH at a Scan Rate of 5 mV s^{-1}

sample	C_s in 1 M H_2SO_4 (F g^{-1})	C_i in 1 M H_2SO_4 (F m^{-2})	C_s in 6 M KOH (F g^{-1})	C_i in 6 M KOH (F m^{-2})
NPSiDC-1	144	0.31	318	0.67
NPSiDC-2	169	0.74	213	0.93
NPSiDC-3	66	0.28	24	0.10

Raman Spectroscopy. Raman spectra of a typical NPSiDC can be seen in Figure 5. As seen from Figure 5, NPSiDC-2 exhibits characteristic D band and G band at 1331 and 1605 cm^{-1}, respectively. The D band, also called disordered band is due to breathing mode of sp^2 carbons attached to a series of defects whereas the G band, also called graphitic band is due to the stretching motion of sp^2 carbon atoms.[44,45] The ratio of intensities of D band and G band reflects the extent of disordered carbon.[2] The I_D/I_G value for NPSiDC-2 was found to be 1.21.

Four Point Probe Conductivity Measurements. Table 7 shows the bulk conductivity values of NPSiDCs blended with 20% PTFE (polytetrafluoroethylene). NPSiDC-1 exhibits better conductivity values whereas NPSiDC-2 and NPSiDC-3 were observed to be hardly conductive. The measurements were recorded at three different spots on pellet prepared from each sample and an average of observed conductivity values have been reported.

Electrochemical Analysis. Cyclic voltammograms of NPSiDCs recorded in 1 M H_2SO_4 at a scan rate of 5 mV s^{-1} in a potential range of 0 to 800 mV can be seen in Figure 6.

DOI: 10.1021/acssuschemeng.5b00453
ACS Sustainable Chem. Eng. 2015, 3, 2194−2202

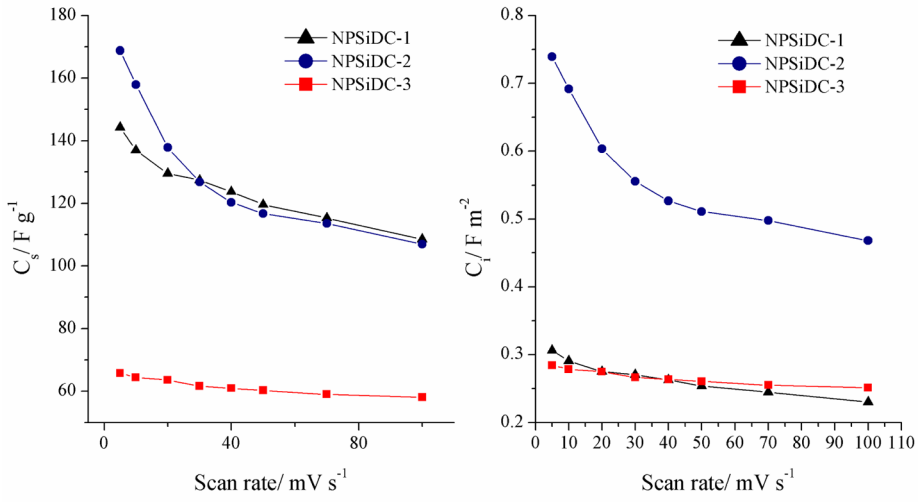

Figure 8. Effect of scan rate on C_s and C_i of NPSiDCs in 1 M H_2SO_4.

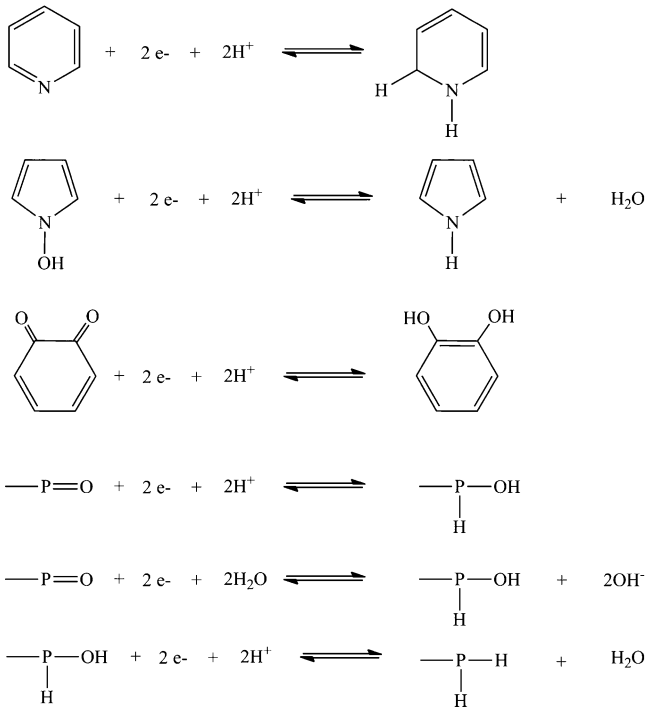

Figure 9. Possible faradaic redox reactions involving N, O, and P functionalities.

The shapes of the voltammograms are almost rectangular indicating significant contribution from electrical double layer capacitance (EDLC). Also, it is evident that the current density due to NPSiDC-2 is more than that due to NPSiDC-1 and NPSiDC-3 and hence the following trend in specific capacitance (C_s) values in 1 M H_2SO_4: NPSiDC-2 > NPSiDC-1 > NPSiDC-3. The high specific capacitance value of NPSiDC-2 over NPSiDC-1 and NPSiDC-3 can be attributed to its surface area, presence of micropores, mesopores, macropores, good dopant concentration and electrical conductivity. Also, broad humps (prominent with NPSiDC-2) were observed in the potential range of 0.1 to 0.5 V. This can be due to pseudocapacitive faradaic redox reactions occurring on the surface of the electrode material. The cyclic voltammograms of NPSiDC-1, NPSiDC-2, and NPSiDC-3 recorded at different

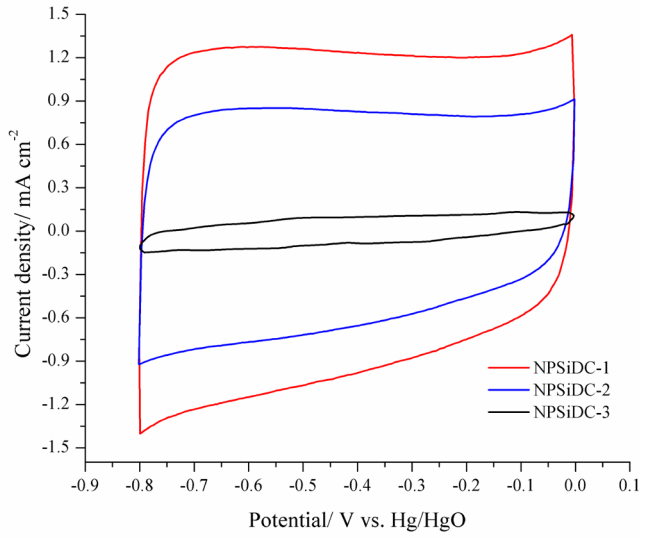

Figure 10. Cyclic voltammograms of NPSiDCs recorded in 6 M KOH at a scan rate of 5 mV s^{-1}.

scan rates ranging from 5 to 100 mVs^{-1} in a potential range of 0 to 800 mV in 1 M H_2SO_4 can be seen in Figures S7, 7, and S8, respectively. The C_s and C_i values for NPSiDCs in 1 M H_2SO_4 determined from cyclic voltammograms recorded at a scan rate of 5 mV s^{-1} can be seen in Table 8.

Figure 8 demonstrates the effect of scan rate on C_s and C_i values calculated from cyclic voltammograms recorded at different scan rates in 1 M H_2SO_4. As expected, it is observed that current density increased with increase in scan rate. However, the C_s values decreased, which is due to the fact that as scan rate increases the ion accessible electroactive surface material decreases and hence the decrease in C_s.[4,46] NPSiDC-1 suffered a 25% loss in C_s whereas NPSiDC-2 and NPSiDC-3 suffered a 37% and 12% loss in C_s respectively as the scan rate increased from 5 to 100 mV s^{-1}. Therefore, it is evident that in the case of NPSiDC-1 and NPSiDC-3, there is better penetration of ions into the electrode material at higher scan rates compared to NPSiDC-2.

As already discussed, pseudocapacitance (PC) is due to redox reactions between ions in the electrolyte and doped functionalities like N, O, and P on the surface of the electrode

DOI: 10.1021/acssuschemeng.5b00453
ACS Sustainable Chem. Eng. 2015, 3, 2194−2202

material. All NPSiDCs have N, O, and P functionalities on the surface as evidenced from XPS results. Pyridinic and pyrrolic Ns can undergo redox reactions in the presence of protons and generate PC. Oxygen dopants in the form of quinone can get reduced to hydroquinone in acidic environment. Phosphorus, similar to N in its electronic character, having a lone pair of electrons, can interact readily with positively charged species like protons resulting in PC. Figure 9 lists possible electrochemical redox reactions involving heteroatom dopants like N, O, and P.

Similarly, cyclic voltammograms of NPSiDCs were also recorded in 6 M KOH. Figure 10 shows the recorded cyclic voltammograms of NPSiDCs recorded at a scan rate of 5 mVs^{-1} in 6 M KOH in a potential range of −0.8 V to 0. It is evident from Figure 10 that the current density due to NPSiDC-1 is significantly greater than that due to NPSiDC-2 and NPSiDC-3 and hence the following observed trend in their C_s values: NPSiDC-1 > NPSiDC-2 > NPSiDC-3. The unusually high C_s value of NPSiDC-1 over other NPSiDCs can be attributed to its high surface area, presence of micropores, mesopores, and macropores, and presence of dopants. On the contrary, NPSiDC-3 exhibits a low C_s value. This can be due to the high concentration of dopants like Si (which decreases electrical conductivity), less surface area and improper carbonization (as seen from the gray color of the product resulting in non-conductive carbon). Also, in the case of NPSiDC-1 and NPSiDC-2, small broad humps (deviation from perfect rectangular shape) can be seen in the potential range of about −0.8 to −0.5 V. These broad humps can be attributed to faradaic redox reactions occurring on the surface of electrode materials leading to PC generation. Also, the cyclic voltammograms were recorded at different scan rates ranging from 5 to 100 mVs^{-1} for NPSiDCs in a potential range of −0.8 V−0. Figures 11, S9, and S10 represent the cyclic voltammograms of NPSiDC-1, NPSiDC-2, and NPSiDC-3 recorded at different scan rates in 6 M KOH. It is evident that as the scan rate increased current density increased, as expected. The C_s and C_i values for NPSiDCs recorded in 6 M KOH at a scan rate of 5 mV s^{-1} can be seen in Table 8 reported earlier.

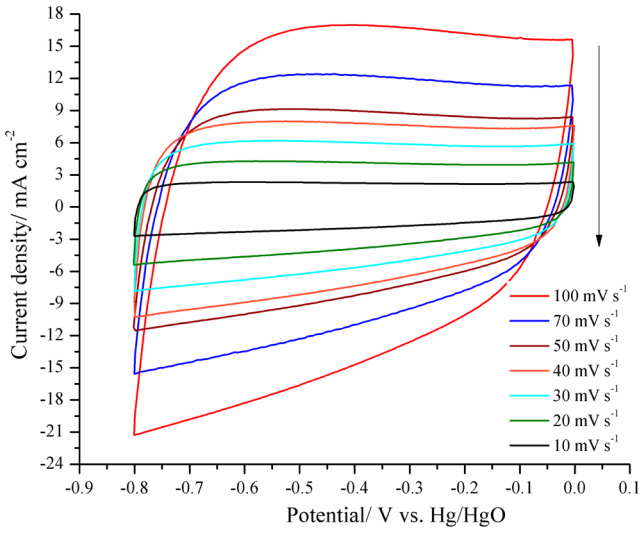

Figure 11. Cyclic voltammograms of NPSiDC-1 recorded in 6 M KOH at different scan rates.

From the cyclic voltammograms recorded at different scan rates in 6 M KOH, C_s and C_i values were calculated based on the equations reported earlier and the effect of scan rate on C_s and C_i values was investigated. It was noticed that as the scan rate increased current density increased but C_s decreased as the ion accessible electroactive surface material decreases.[4,46] As a result NPSiDC-1, NPSiDC-2, and NPSiDC-3 suffered a 32%, 30%, and 44% loss in C_s, respectively, as the scan rate increased from 5 to 100 mV s^{-1}. NPSiDC-1 and NPSiDC-2 suffered less loss in C_s as the scan rate increased from 5 to 100 mV s^{-1} (compared to NPSiDC-3) which can be attributed to better penetration of ions through the pores of the electrode material at higher scan rates. Figure 12 shows a plot of C_s and C_i values of NPSiDCs against scan rate.

An electrochemical stability test was performed by generating 2000 continuous cyclic voltammograms for NPSiDC-2 in 6 M KOH at a scan rate of 5 mV s^{-1}. The cyclic voltammograms recorded in 6 M KOH at a scan rate of 5 mV s^{-1} before and after recording continuous 2000 cyclic voltammograms were compared and are reported in Figure 13. As seen from Figure 13, NPSiDC-2 was observed to be highly stable over 2000 cycles in 6 M KOH.

Figure 14 illustrates the charge−discharge studies of NPSiDCs recorded in 6 M KOH at a current density of 0.2 A g^{-1}. The charge−discharge curves of NPSiDC-1 are asymmetric

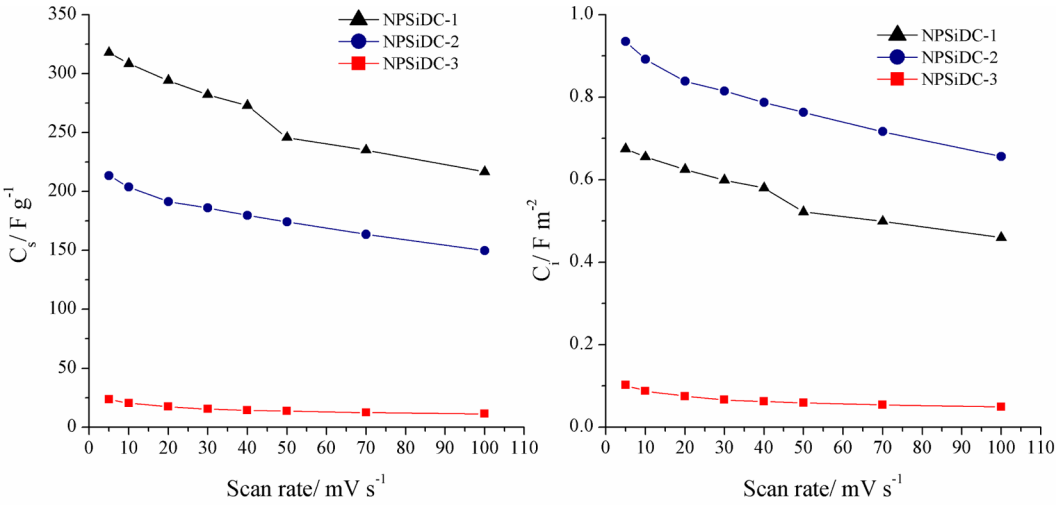

Figure 12. Effect of scan rate on C_s and C_i of NPSiDCs in 6 M KOH.

DOI: 10.1021/acssuschemeng.5b00453
ACS Sustainable Chem. Eng. 2015, 3, 2194−2202

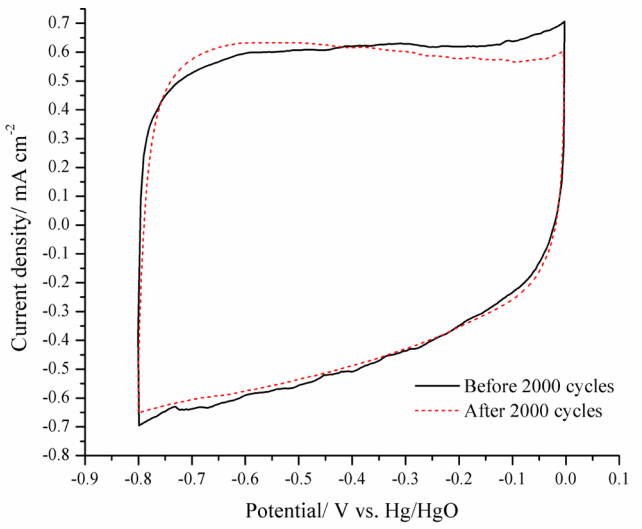

Figure 13. Cyclic voltammograms of NPSiDC-2 in 6 M KOH before and after recording continuous 2000 cycles at a scan rate of 5 mV s^{-1}.

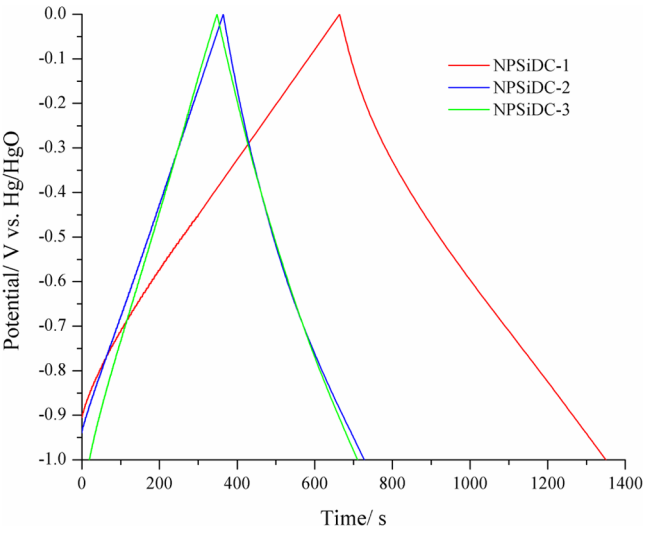

Figure 14. Galvanostatic charge−discharge curves of NPSiDCs recorded in 6 M KOH at a current density of 0.2 A g^{-1}.

toward lower potential values indicating contribution from pseudocapacitance. Beyond 0 V, significant curvature in the charge−discharge branch appears may be due to the oxidation of electrode material.[17] The maximum operating voltage of 1 V for NPSiDCs corresponds with the maximum operating voltage for many porous carbon materials.[33,47]

SUMMARY OF WORK

Three different kinds of NPSiDCs were developed from thiamine as the renewable resource material employing a novel microwave-assisted method. The method is simple, rapid, and inexpensive, which does not employ any reducing gases and is relatively high yielding.

NPSiDC-1 was found to contain high specific surface area of 471 m^2 g^{-1} and single point total pore volume of 0.25 cm^3 g^{-1}. XPS revealed the presence of N, P, and Si defects in C in all NPSiDCs. All NPSiDCs were found to contain pyridinic and graphitic Ns which are believed to play an important role in PC faradaic redox reactions.

NPSiDC-1 and NPSiDC-2 exhibited potential for supercapacitor applications with NPSiDC-1 generating highest specific capacitance value of 318 F g^{-1} in 6 M KOH. NPSiDC-2 was discovered to be electrochemically stable in 6 M KOH where hardly any loss in specific capacitance was observed even after recording 2000 continuous cycles.

ASSOCIATED CONTENT

Supporting Information

The Supporting Information is available free of charge on the ACS Publications website at DOI: 10.1021/acssuschemeng.5b00453.

Figures S1−S10 as mentioned in the text (PDF)

AUTHOR INFORMATION

Corresponding Authors

*E-mail: sxramasahaya@ualr.edu (S.K.R.).
*E-mail: txviswanatha@ualr.edu (T.V.).

Notes

The authors declare no competing financial interest.

ACKNOWLEDGMENTS

The authors would like to thank Dr. Shawn Bourdo, Dr. Viney, Saini, and Dr. Zeid Nima at Centre for Integrative Nanotechnology Sciences, University of Arkansas, at Little Rock for help with characterization of NPSiDCs. The authors would also like to acknowledge the partial financial support received through NASA Research Infrastructure Development grant.

REFERENCES

(1) Xiong, W.; Liu, M.; Gan, L.; Lv, Y.; Li, Y.; Yang, L.; Xu, Z.; Hao, Z.; Liu, H.; Chen, L. A novel synthesis of mesoporous carbon microspheres for supercapacitor electrodes. *J. Power Sources* **2011**, *196* (23), 10461−10464.

(2) Liu, M.; Gan, L.; Xiong, W.; Xu, Z.; Zhu, D.; Chen, L. Development of MnO2/porous carbon microspheres with a partially graphitic structure for high performance supercapacitor electrodes. *J. Mater. Chem. A* **2014**, *2* (8), 2555−2562.

(3) Wang, G.; Zhang, L.; Zhang, J. A review of electrode materials for electrochemical supercapacitors. *Chem. Soc. Rev.* **2012**, *41* (2), 797−828.

(4) Wang, D.-W.; Li, F.; Chen, Z.-G.; Lu, G. Q.; Cheng, H.-M. Synthesis and Electrochemical Property of Boron-Doped Mesoporous Carbon in Supercapacitor. *Chem. Mater.* **2008**, *20* (22), 7195−7200.

(5) Jiang, H.; Lee, P. S.; Li, C. 3D carbon based nanostructures for advanced supercapacitors. *Energy Environ. Sci.* **2013**, *6* (1), 41−53.

(6) Gopalakrishnan, K.; Moses, K.; Govindaraj, A.; Rao, C. N. R. Supercapacitors based on nitrogen-doped reduced graphene oxide and borocarbonitrides. *Solid State Commun.* **2013**, *175−176*, 43−50.

(7) Zhang, Y.; Feng, H.; Wu, X.; Wang, L.; Zhang, A.; Xia, T.; Dong, H.; Li, X.; Zhang, L. Progress of electrochemical capacitor electrode materials: A review. *Int. J. Hydrogen Energy* **2009**, *34* (11), 4889−4899.

(8) Kotz, R.; Carlen, M. Principles and applications of electrochemical capacitors. *Electrochim. Acta* **2000**, *45* (15−16), 2483−2498.

(9) Wan, L.; Wang, J.; Xie, L.; Sun, Y.; Li, K. Nitrogen-Enriched Hierarchically Porous Carbons Prepared from Polybenzoxazine for High-Performance Supercapacitors. *ACS Appl. Mater. Interfaces* **2014**, *6* (17), 15583−15596.

(10) Yan, X.; Liu, Y.; Fan, X.; Jia, X.; Yu, Y.; Yang, X. Nitrogen/phosphorus co-doped nonporous carbon nanofibers for high-performance supercapacitors. *J. Power Sources* **2014**, *248*, 745−751.

(11) Wang, C.; Sun, L.; Zhou, Y.; Wan, P.; Zhang, X.; Qiu, J. P/N co-doped microporous carbons from H3PO4-doped polyaniline by in situ activation for supercapacitors. *Carbon* **2013**, *59*, 537−546.

DOI: 10.1021/acssuschemeng.5b00453
ACS Sustainable Chem. Eng. 2015, 3, 2194−2202

(12) Li, X.; Wang, H.; Robinson, J. T.; Sanchez, H.; Diankov, G.; Dai, H. Simultaneous Nitrogen Doping and Reduction of Graphene Oxide. *J. Am. Chem. Soc.* **2009**, *131* (43), 15939−15944.
(13) Wang, H.; Xu, Z.; Kohandehghan, A.; Li, Z.; Cui, K.; Tan, X.; Stephenson, T. J.; King'ondu, C. K.; Holt, C. M. B.; Olsen, B. C.; Tak, J. K.; Harfield, D.; Anyia, A. O.; Mitlin, D. Interconnected Carbon Nanosheets Derived from Hemp for Ultrafast Supercapacitors with High Energy. *ACS Nano* **2013**, *7* (6), 5131−5141.
(14) Rufford, T. E.; Hulicova-Jurcakova, D.; Zhu, Z.; Lu, G. Q. Nanoporous carbon electrode from waste coffee beans for high performance supercapacitors. *Electrochem. Commun.* **2008**, *10* (10), 1594−1597.
(15) Prasad, K. S.; Pallela, R.; Kim, D.-M.; Shim, Y.-B. Microwave-Assisted One-Pot Synthesis of Metal-Free Nitrogen and Phosphorus Dual-Doped Nanocarbon for Electrocatalysis and Cell Imaging. *Particle & Particle Systems Characterization* **2013**, *30* (6), 557−564.
(16) Sun, L.; Wang, L.; Tian, C.; Tan, T.; Xie, Y.; Shi, K.; Li, M.; Fu, H. Nitrogen-doped graphene with high nitrogen level via a one-step hydrothermal reaction of graphene oxide with urea for superior capacitive energy storage. *RSC Adv.* **2012**, *2* (10), 4498−4506.
(17) Ania, C. O.; Khomenko, V.; Raymundo-Pinero, E.; Parra, J. B.; Beguin, F. The large electrochemical capacitance of microporous doped carbon obtained by using a zeolite template. *Adv. Funct. Mater.* **2007**, *17* (11), 1828−1836.
(18) Dong, X.-C.; Xu, H.; Wang, X.-W.; Huang, Y.-X.; Chan-Park, M. B.; Zhang, H.; Wang, L.-H.; Huang, W.; Chen, P. 3D Graphene-Cobalt Oxide Electrode for High-Performance Supercapacitor and Enzymeless Glucose Detection. *ACS Nano* **2012**, *6* (4), 3206−3213.
(19) Panchakarla, L. S.; Subrahmanyam, K. S.; Saha, S. K.; Govindaraj, A.; Krishnamurthy, H. R.; Waghmare, U. V.; Rao, C. N. R. Synthesis, Structure, and Properties of Boron- and Nitrogen-Doped Graphene. *Adv. Mater.* **2009**, *21* (46), 4726−4730.
(20) Wei, D.; Liu, Y.; Wang, Y.; Zhang, H.; Huang, L.; Yu, G. Synthesis of N-Doped Graphene by Chemical Vapor Deposition and Its Electrical Properties. *Nano Lett.* **2009**, *9* (5), 1752−1758.
(21) Xu, B.; Hou, S.; Cao, G.; Wu, F.; Yang, Y. Sustainable nitrogen-doped porous carbon with high surface areas prepared from gelatin for supercapacitors. *J. Mater. Chem.* **2012**, *22* (36), 19088−19093.
(22) Ramasahayam, S. K.; Gunawan, G.; Finlay, C.; Viswanathan, T. Renewable resource-based magnetic nanocomposites for removal and recovery of phosphorous from contaminated waters. *Water, Air, Soil Pollut.* **2012**, *223* (8), 4853−4863.
(23) Viswanathan, T. Doped-carbon composites, synthesizing methods and applications of the same. Patent 2013-13767076 20130157838, 20130214, 2013.
(24) Viswanathan, T. Renewable resource-based metal oxide-containing materials and applications. Patent 2013-13843106 20130233802, 20130315, 2013.
(25) Bairi, V. G.; Bourdo, S. E.; Nasini, U. B.; Ramasahayam, S. K.; Watanabe, F.; Berry, B. C.; Viswanathan, T. Microwave-assisted synthesis of nitrogen and phosphorus co-doped mesoporous carbon and their potential application in alkaline fuel cells. *Sci. Adv. Mater.* **2013**, *5* (9), 1275−1281.
(26) Ramasahayam, S. K.; Nasini, U. B.; Bairi, V.; Shaikh, A. U.; Viswanathan, T. Microwave assisted synthesis and characterization of silicon and phosphorous co-doped carbon as an electrocatalyst for oxygen reduction reaction. *RSC Adv.* **2014**, *4* (12), 6306−6313.
(27) Rao, K. J.; Vaidhyanathan, B.; Ganguli, M.; Ramakrishnan, P. A. Synthesis of Inorganic Solids Using Microwaves. *Chem. Mater.* **1999**, *11* (4), 882−895.
(28) Syed, A. A.; Dinesan, M. K. Review: polyaniline a novel polymeric material. *Talanta* **1991**, *38* (8), 815−37.
(29) Sing, K. S. W.; Everett, D. H.; Haul, R. A. W.; Moscou, L.; Pierotti, R. A.; Rouquerol, J.; Siemieniewska, T. Reporting physisorption data for gas/solid systems with special reference to the determination of surface area and porosity. *Pure Appl. Chem.* **1985**, *57* (4), 603−19.
(30) Lv, Y.; Gan, L.; Liu, M.; Xiong, W.; Xu, Z.; Zhu, D.; Wright, D. S. A self-template synthesis of hierarchical porous carbon foams based on banana peel for supercapacitor electrodes. *J. Power Sources* **2012**, *209*, 152−157.
(31) Ma, X.; Liu, M.; Gan, L.; Zhao, Y.; Chen, L. Synthesis of micro- and mesoporous carbon spheres for supercapacitor electrode. *J. Solid State Electrochem.* **2013**, *17* (8), 2293−2301.
(32) Chen, Z.; Higgins, D.; Chen, Z. Nitrogen doped carbon nanotubes and their impact on the oxygen reduction reaction in fuel cells. *Carbon* **2010**, *48* (11), 3057−3065.
(33) Chen, X. Y.; Chen, C.; Zhang, Z. J.; Xie, D. H.; Deng, X.; Liu, J. W. Nitrogen-doped porous carbon for supercapacitor with long-term electrochemical stability. *J. Power Sources* **2013**, *230*, 50−58.
(34) Jeyabharathi, C.; Venkateshkumar, P.; Rao, M. S.; Mathiyarasu, J.; Phani, K. L. N. Nitrogen-doped carbon black as methanol tolerant electrocatalyst for oxygen reduction reaction in direct methanol fuel cells. *Electrochim. Acta* **2012**, *74*, 171−175.
(35) Cheng, W.; Weng, L.-T.; Li, Y.; Lau, A.; Chan, C. K.; Chan, C.-M. Surface Chemical Composition of Size-Fractionated Urban Walkway Aerosols Determined by X-Ray Photoelectron Spectroscopy. *Aerosol Sci. Technol.* **2013**, *47* (10), 1118−1124.
(36) Zhao, X.; Zhang, Q.; Zhang, B.; Chen, C.-M.; Wang, A.; Zhang, T.; Su, D. S. Dual-heteroatom-modified ordered mesoporous carbon: Hydrothermal functionalization, structure, and its electrochemical performance. *J. Mater. Chem.* **2012**, *22* (11), 4963−4969.
(37) Zhao, X.; Wang, A.; Yan, J.; Sun, G.; Sun, L.; Zhang, T. Synthesis and Electrochemical Performance of Heteroatom-Incorporated Ordered Mesoporous Carbons. *Chem. Mater.* **2010**, *22* (19), 5463−5473.
(38) Jeong, H. M.; Lee, J. W.; Shin, W. H.; Choi, Y. J.; Shin, H. J.; Kang, J. K.; Choi, J. W. Nitrogen-doped graphene for high-performance ultracapacitors and the importance of nitrogen-doped sites at basal planes. *Nano Lett.* **2011**, *11* (6), 2472−2477.
(39) Wang, C.; Zhou, Y.; Sun, L.; Wan, P.; Zhang, X.; Qiu, J. Sustainable synthesis of phosphorus- and nitrogen-co-doped porous carbons with tunable surface properties for supercapacitors. *J. Power Sources* **2013**, *239*, 81−88.
(40) Choi, C. H.; Park, S. H.; Woo, S. I. Binary and Ternary Doping of Nitrogen, Boron, and Phosphorus into Carbon for Enhancing Electrochemical Oxygen Reduction Activity. *ACS Nano* **2012**, *6* (8), 7084−7091.
(41) Wickramaratne, N. P.; Xu, J.; Wang, M.; Zhu, L.; Dai, L.; Jaroniec, M. Nitrogen Enriched Porous Carbon Spheres: Attractive Materials for Supercapacitor Electrodes and CO2 Adsorption. *Chem. Mater.* **2014**, *26* (9), 2820−2828.
(42) Wei, J.; Zhou, D.; Sun, Z.; Deng, Y.; Xia, Y.; Zhao, D. A Controllable Synthesis of Rich Nitrogen-Doped Ordered Mesoporous Carbon for CO2 Capture and Supercapacitors. *Adv. Funct. Mater.* **2013**, *23* (18), 2322−2328.
(43) Liu, Z.; Fu, X.; Li, M.; Wang, F.; Wang, Q.; Kang, G.; Peng, F. Novel silicon-doped, silicon and nitrogen-codoped carbon nanomaterials with high activity for the oxygen reduction reaction in alkaline medium. *J. Mater. Chem. A* **2015**, *3* (7), 3289−3293.
(44) Liu, M.; Gan, L.; Xiong, W.; Zhao, F.; Fan, X.; Zhu, D.; Xu, Z.; Hao, Z.; Chen, L. Nickel-Doped Activated Mesoporous Carbon Microspheres with Partially Graphitic Structure for Supercapacitors. *Energy Fuels* **2013**, *27* (2), 1168−1173.
(45) Ramasahayam, S. K.; Nasini, U. B.; Shaikh, A. U.; Viswanathan, T. Novel tannin-based Si, P co-doped carbon for supercapacitor applications. *J. Power Sources* **2015**, *275*, 835−844.
(46) Nasini, U. B.; Bairi, V. G.; Ramasahayam, S. K.; Bourdo, S. E.; Viswanathan, T.; Shaikh, A. U. Phosphorous and nitrogen dual heteroatom doped mesoporous carbon synthesized via microwave method for supercapacitor application. *J. Power Sources* **2014**, *250*, 257−265.
(47) Ma, C.; Shi, J.; Song, Y.; Zhang, D.; Zhai, X.; Zhong, M.; Guo, Q.; Liu, L. Preparation and capacitive properties of nitrogen-enriched hierarchical porous carbon. *Int. J. Electrochem. Sci.* **2012**, *7* (8), 7587−7599.

DOI: 10.1021/acssuschemeng.5b00453
ACS Sustainable Chem. Eng. 2015, 3, 2194−2202